Available online at www.sciencedirect.com
ScienceDirect
Trans. Nonferrous Met. Soc. China 32(2022) 3790−3800
Transactions of Nonferrous Metals Society of China
www.tnmsc.cn

Molten salt electrosynthesis of silicon carbide nanoparticles and their photoluminescence property

Zhong-ya PANG[1], Xiang LI[1], Xue-qiang ZHANG[1], Jin-jian LI[1], Shu-juan WANG[1], Xiao-lu XIONG[1], Guang-shi LI[1], Qian XU[1], Zhong-fu ZHOU[1,2], Xing-li ZOU[1], Xiong-gang LU[1,3]

1. State Key Laboratory of Advanced Special Steel & Shanghai Key Laboratory of Advanced Ferrometallurgy, School of Materials Science and Engineering, Shanghai University, Shanghai 200444, China;
2. Institute of Mathematics and Physics, Aberystwyth University, Aberystwyth SY23 3BZ, UK;
3. School of Materials Science, Shanghai Dianji University, Shanghai 201306, China

Received 12 September 2021; accepted 19 January 2022

Abstract: A one-step molten salt electrochemical strategy was proposed to synthesize SiC nanoparticles from ultra-fine silicon dioxide/carbon (SiO_2/C) mixtures. The electrosynthesis process and physicochemical properties of the synthesized products were systematically analyzed via X-ray diffraction, electron microscopy, Raman spectroscopy and photoluminescence spectroscopy, etc. A combined chemical/electrochemical reaction, electrochemical deoxidation, and in-situ carbonization reaction mechanism was proposed to reveal the electrochemical synthesis process of SiC nanoparticles from SiO_2/C in molten $CaCl_2$. The as-prepared SiC with particle size ranging from 8 to 14 nm possesses a polycrystalline structure. In addition, the SiC nanoparticles demonstrate obvious photoluminescence property due to the synergetic size effect and microstructural characteristics.

Key words: SiC; nanomaterials; molten salt electrosynthesis; deoxidation; photoluminescence

1 Introduction

In recent years, semiconductor nanomaterials present wide application prospects in the fields of biological detection, photovoltaic conversion, and data-storage, etc, due to their unique electrical, optical, and mechanical properties. Silicon carbide (SiC), as a representative third-generation wide bandgap semiconductor material, possesses numerous outstanding properties [1,2], such as high thermal conductivity (4.9 $W \cdot cm^{-1} \cdot K^{-1}$), high saturated electron mobility (2.0×10^7 cm/s), high breakdown field strength (3.0 MV/cm), good anti-radiation ability (10^5 W/cm^2), and high thermal stability. As the size of SiC decreases to the nanometer range, certain photoelectric properties can be induced or enhanced due to its size effects [1], and SiC nanomaterials can be used in wider fields. For instance, SiC nanomaterial has been considered to be a good candidate for blue and ultraviolet luminescent displays due to its intensified luminescent properties [3]. Besides, SiC nanoparticles with better compatibility and transmission capability may present exciting opportunities for biomarkers and medicines [4].

To date, various synthetic techniques have been proposed and applied to the preparation of SiC nanomaterials, such as carbothermal reduction of the silicon/carbon-containing precursors [5,6],

Corresponding author: Xiao-lu XIONG, Tel: +86-21-66136518, E-mail: xlxiong@t.shu.edu.cn;
Xing-li ZOU, Tel: +86-21-66136518, E-mail: xlzou@shu.edu.cn;
Xiong-gang LU, Tel: +86-21-66136518, E-mail: luxg@shu.edu.cn
DOI: 10.1016/S1003-6326(22)66058-8

chemical vapor deposition [7], laser pyrolysis and ablation [8], and high energy ball milling [3]. Even though ultra-fine SiC powder can be synthesized via these methods, the complex procedures and/or high costs are some of the most concerning obstacles in development and commercialization of these preparation techniques. Thus, exploring alternative methods to prepare SiC nanomaterials are still extremely needed.

Molten salt electrolysis is a versatile and sustainable technology that can rely on electrons to purify and prepare functional materials without additional redox agents [9−11]. In recent years, with the development of molten salt electrochemical strategy represented by the FFC-Cambridge process, a variety of metals, alloys, and semiconductor materials have been electrochemically synthesized from their corresponding metal oxides [10−12]. In general, the advantages of molten salt electrolysis include: (1) The production process of metal/alloy/semiconductor materials is simplified by using readily available and low-cost oxides as raw materials; (2) The electrolysis temperature is relatively low, generally 700−900 °C, which can reduce energy consumption; (3) The synthesized product with diverse and controllable morphology has high added value. For the synthesis of Si-based nanomaterials, the previous researches confirmed that low-metal property and intrinsic orientation-growth mechanism of silicon materials can provoke the formation of micro/nano-structures during the molten salt electrosynthesis process [12,13]. Meanwhile, thermodynamic spontaneous reaction of silicon and carbon provides convenience to the electrochemical synthesis of ultra-fine SiC nanomaterials [12].

In this work, homogeneous SiC nanoparticles were prepared directly from silicon dioxide/carbon mixtures in molten calcium chloride ($CaCl_2$) via a one-step electrochemical synthetic strategy. The phase evolution, element composition, and morphological change of the cathodic products were systematically investigated. A possible formation mechanism of SiC nanoparticles was proposed according to the experimental results. Furthermore, the microstructural characteristics and room-temperature photoluminescence property of the resultant SiC nanoparticles were also investigated.

2 Experimental

2.1 Fabrication of electrodes

SiO_2 and carbon (C) powder with the average particle sizes of 15 nm and 10 nm, respectively, were purchased from Shanghai Macklin Biochemical Co., Ltd. (China). SiO_2 and C powders (in a molar ratio of Si:C=1:1), and 15 wt.% polyvinyl butyral (PVB) were well mixed using a planetary muller at 250 r/min for 5 h. Approximately 0.4 g mixture was compressed in a stainless-steel mold under a pressure of 20 MPa to fabricate a SiO_2/C pellet with a diameter of 10 mm. The obtained SiO_2/C pellet was subsequently wrapped with porous nickel foam and fastened to a molybdenum wire (2 mm in diameter). The assembled SiO_2/C electrode was used as a cathode for the synthesis of SiC. A high-purity graphite rod with a diameter of 10 mm served as the anode.

2.2 Molten salt electrolysis experiments

Anhydrous $CaCl_2$ (Shanghai Aladdin Co., Ltd. (China)) used as the electrolyte was first dried at 400 °C for 24 h. SiO_2/C cathode, graphite anode, and the pre-treated $CaCl_2$ were assembled into a corundum crucible to form the electrolytic cell, which was subsequently placed in electrolytic furnace for synthesis of SiC. The schematic illustration of the electrolytic cell as well as the furnace is shown in Fig. 1. The electrolytic cell was protected by continuously injected argon gas (99.9999%) during the entire experiment. When the furnace temperature reached 900 °C, pre-electrolysis was conducted between two graphite electrodes (10 mm in diameter) at a constant potential of 2.5 V to eliminate the possible residual moisture in $CaCl_2$. A constant potential of 3.0 V was applied between the SiO_2/C cathode and graphite anode by the electrochemical workstation or constant voltage power supply. As the electrolysis reached the designated time, electrolysis was halted and the cathodic product was cooled to room temperature with the furnace at the cooling rate of 2 °C/min. Deionized water were used to clean the residual solid salt and possible impurities. The resultant products were then dried at 100 °C in air for the subsequent analyses. Cyclic voltammetry measurement was performed to investigate the electro-reduction process, where the metallic Mo

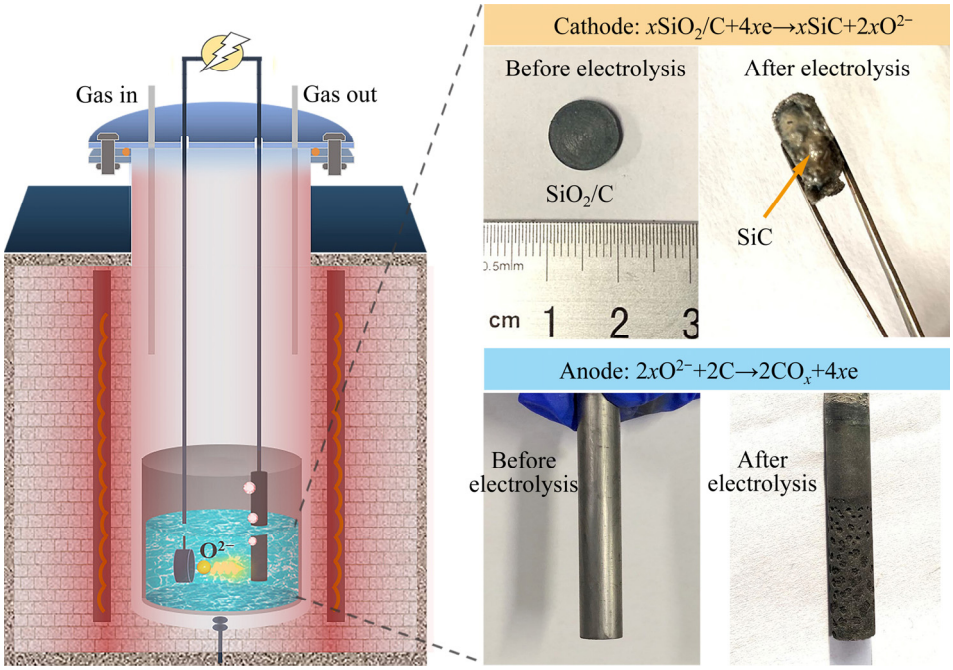

Fig. 1 Schematic illustration of electrolytic cell and furnace, as well as digital photographs of cathode and graphite anode before and after electrolysis

cavity electrode (with width of 5 mm, thickness of 1.5 mm, and cavity diameter of 1 mm) loaded with SiO_2/C powder, platinum wire (1 mm in diameter), and graphite rod (10 mm in diameter) were used as working electrode, reference electrode, and counter electrode, respectively.

2.3 Characterizations

X-ray diffraction (XRD, D8 Advance, Bruker) was used to determine the phase composition of the electrolytic products. Scanning electron microscopy (SEM, FEI Nova Nanosem 450) and energy-dispersive X-ray spectroscopy (EDS) were utilized to analyze the morphology and element composition of the products, respectively. The microstructures of the products were further characterized by transmission electron microscopy (TEM, FEI Tecnai G2 F20). Renishaw inVia Raman microspectrometer with 355 nm Ar ion laser was used to analyze the resultant SiC nanoparticles. Photoluminescence spectrum of the synthesized SiC was collected using a Hitachi F−7100 luminescence spectrofluorometer with an excitation wavelength of 252 nm. The thermodynamic data were calculated by HSC chemistry version 6.0. The current-time and CV curves were recorded by a Princeton P4000 electrochemical workstation. The current efficiency (η) was calculated by the following equation:

$$\eta=\frac{nFm}{CM}\times 100\% \quad (1)$$

where n represents the number of transferred electrons; F represents Faraday constant; m represents the actual mass of the Si (70% of the mass of the synthesized SiC); C represents the total charge in the electrolysis process; M represents the relative atomic mass of Si.

3 Results and discussion

3.1 Electrosynthesis of SiC from SiO_2/C

The current−time curve of the electrosynthesis of SiC from SiO_2/C in molten $CaCl_2$ at 900 °C and 3.0 V is shown in Fig. 2(a). It is obvious that the current decreases rapidly from about 0.8 to 0.4 A during the initial electrolysis stage, and then it declines gradually to about 0.2 A after 4 h. The current efficiency of the electrolysis process is calculated to be about 49.4%. The variation of the current observed in this work complies with the previous electrochemical deoxidation process of metal oxides-containing cathode systems [14−16]. According to the previous works [9,17], electrochemical deoxidation process followed the propagation of semiconductor (Si)/oxide (SiO_2)/

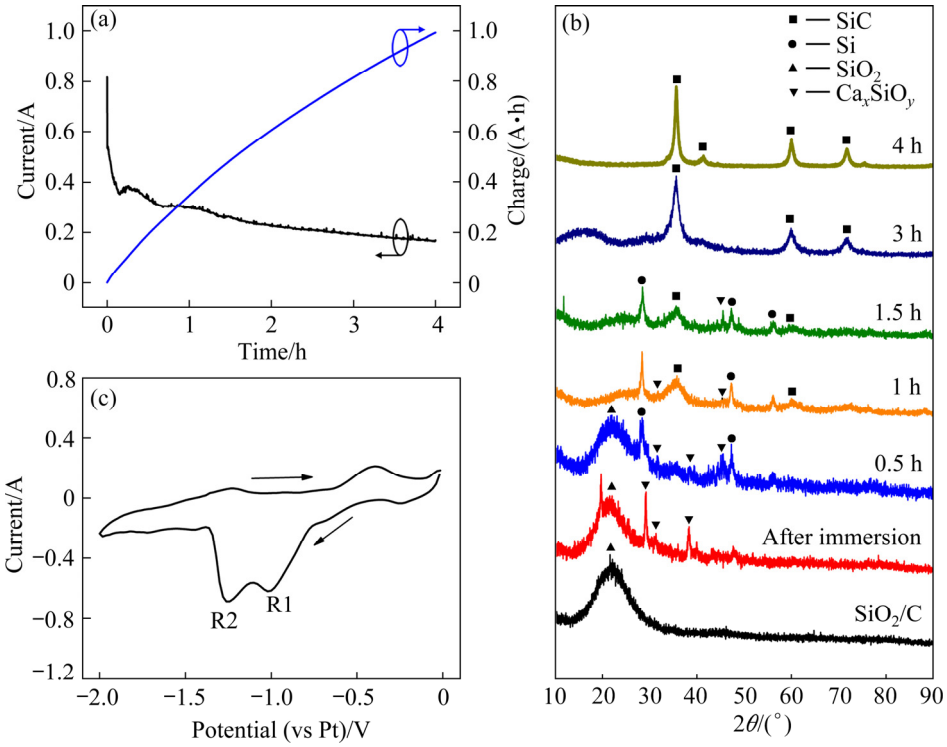

Fig. 2 Current−time curve of electrosynthesis of SiC from SiO_2/C in molten $CaCl_2$ at 900 °C and 3.0 V (a); XRD patterns of SiO_2/C pellets before and after being immersed and electrolyzed in molten $CaCl_2$ for different durations (b); CV curve of SiO_2/C in molten $CaCl_2$ at scan rate of 50 mV/s (c)

electrolyte (molten $CaCl_2$) three-phase interlines (3PIs) in the SiO_2/C pellet. At the initial electrolysis stage, the rapid decrease of current indicates that the SiO_2/C electrode quickly reaches a relatively stable deoxidation process. The latter current platform means that electrochemical deoxidation of SiO_2 in the cathode is gradually completed. The above-mentioned deoxidation and current variation processes are affected by many factors, such as the transfer efficiency of oxygen ions, the porosity and conductivity of generated SiC coating, and the concentration of oxygen ions in the reaction zone and molten salt. Figure 2(b) presents the XRD patterns of the SiO_2/C pellets before and after being immersed and electrolyzed in molten $CaCl_2$ for different durations. The SiO_2/C pellet after being immersed in molten $CaCl_2$ for 5 h exhibits the typical characteristic peaks of silicates (labeled as Ca_xSiO_y, including $CaSiO_3$ and Ca_2SiO_4, etc). The generation of Ca_xSiO_y is due to the thermodynamically spontaneous combination reaction between SiO_2 and CaO (Ca^{2+}, O^{2-}) that exists as hardly removed impurity in molten salt [18,19]. The phase composition of cathodic products further changes after performing electrolysis for 0.5 h. The XRD pattern shows the hybrid peaks of Si, SiO_2, and Ca_xSiO_y, which indicates the progress of electrochemical deoxidation reactions. The characteristic peaks of SiO_2 disappear when the electrolysis duration extends to 1 h, whereas SiC, Si, and Ca_xSiO_y become the dominant phases. The final cathodic product is evidenced as pure SiC phase (PDF #75-0254) after electrolysis for 4 h. Cyclic voltammetry curve recorded at a scan rate of 50 mV/s is shown in Fig. 2(c). According to the CV curve, the electrolysis process of SiO_2/C consists of the electrochemical reduction of SiO_2 (Peak R1) and Ca_xSiO_y (Peak R2). The previous works have confirmed that direct electrochemical reduction of SiO_2 and dissolution−reduction of Ca_xSiO_y coexisted in the electrosynthesis process of SiC [12,13].

Figure 3 shows morphological transformation of the cathodic products during the electrolysis process. SiO_2/C precursor and the cathodic products obtained in the earlier stages, e.g., 0.5 and 1 h, possess a typical black color due to the existence of carbon (Fig. 3(a)). It should be noted that no obvious characteristic peaks of carbon are detected by XRD since amorphous carbon powder

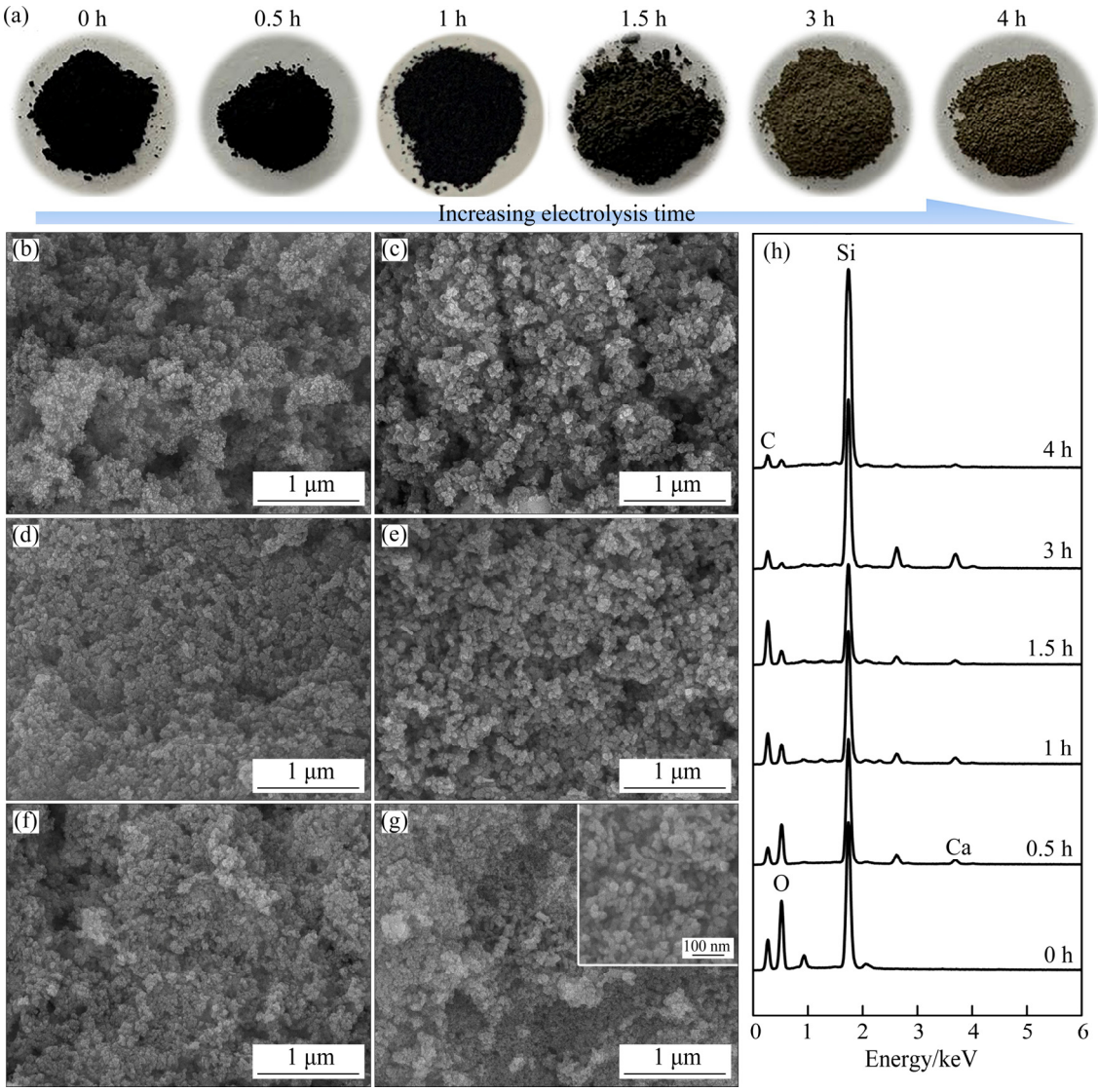

Fig. 3 Digital photographs (a), SEM images (b−g), and their corresponding EDS spectra (h) of cathodic products obtained at different electrolysis durations: (b) 0 h; (c) 0.5 h; (d) 1 h; (e) 1.5 h; (f) 3 h; (g) 4 h

was used in this work. With increasing SiC contents, the color of the cathodic products changes from black to black-grey and to yellow-grey. Furthermore, as evidenced by the digital photograph in Fig. 1, a certain extent of oxidation−corrosion reaction exists on the surface of the anodic graphite rod. These observations indicate the successful electrochemical deoxidation between SiO_2 and Ca_xSiO_y, and the in-situ carbonization reaction between Si and C. Figures 3(b−h) show the SEM images and their corresponding EDS spectra of the cathodic products obtained after different electrolysis durations. The SEM images present that the morphology of the cathodic products has no obvious change, and electrolytic intermediate products (Figs. 3(b−f)) all show the morphology of nano-particles, indicating that the reaction occurs at the nanometer scale. As shown in Fig. 3(g), uniform SiC nanoparticles with particle size of about 10 nm can be obtained. The EDS spectra (Fig. 3(h)) further reveal the effective removal of the oxygen from the cathode. The detection of calcium (Ca) in the EDS spectra of the intermediate products also verifies the existence of Ca_xSiO_y during the electrolysis process, which is consistent with the XRD result.

3.2 Reaction mechanism of electrosynthesis process

To further elucidate the generation mechanism of Ca_xSiO_y and Si, raw $CaCl_2$ without any treatment and $SiO_2/CaCl_2$ mixtures after heating at 900 °C

for 5 h were characterized using XRD, as shown in Fig. 4(a). The result shows that the pristine $CaCl_2$ possesses distinct characteristic peaks that correspond to $CaCl_2$ and $CaCl_2{\cdot}2H_2O$. $CaCl_2{\cdot}2H_2O$ may be introduced from the preparation process of $CaCl_2$ with strong hygroscopicity. Furthermore, calcium silicates (such as $CaSiO_3$ and Ca_2SiO_4) were detected in $SiO_2/CaCl_2$ mixtures after heat-treatment. This result is consistent with that reported in the previous works [20,21], implying that calcium-oxide phase from raw $CaCl_2$ is beneficial to the ionization of silica to form silicate ions through the dissolution and combination processes. DONG et al [22] substantiated that silicate ions could effectively promote the electrochemical reduction rate for the synthesis of silicon. In order to prove that the dissolution−electroreduction process can effectively prepare silicon-based materials, a constant voltage of 3.0 V was subsequently performed on two graphite rods to synthesize Si in the molten $SiO_2/CaCl_2$. Figure 4(b) shows the XRD patterns of the graphite rod serving as cathode before and after electrolysis, and the inset shows the digital photographs of the graphite rod before and after electrolysis. Obvious Si (PDF #77-2107) peaks can be observed in the XRD pattern after performing electrolysis for 30 min, suggesting the successful synthesis of Si from molten SiO_2–$CaCl_2$ via an electrochemical deposition process. This also indicates that the dissolvable silicates generated through liquid-phase reaction in the electrolysis process of SiO_2/C can also be smoothly reduced to solid Si.

Figure 5 shows the SEM images of electrodeposited Si particles. Obviously, the resultant Si possesses a uniform morphology of microspheres with particle size of about 1 μm. By comparison, the size of the electrodeposited Si is sufficiently larger than that of the electrochemically synthesized SiC, as shown in Fig. 3. Such a difference in size is mainly due to the greater ease of nucleation and faster growth behaviors for Si during the electrodeposition process in liquid salt. In addition, the collected EDS mapping, as shown by the inset in Fig. 5(b), further confirms the deposition of Si from the molten $SiO_2/CaCl_2$.

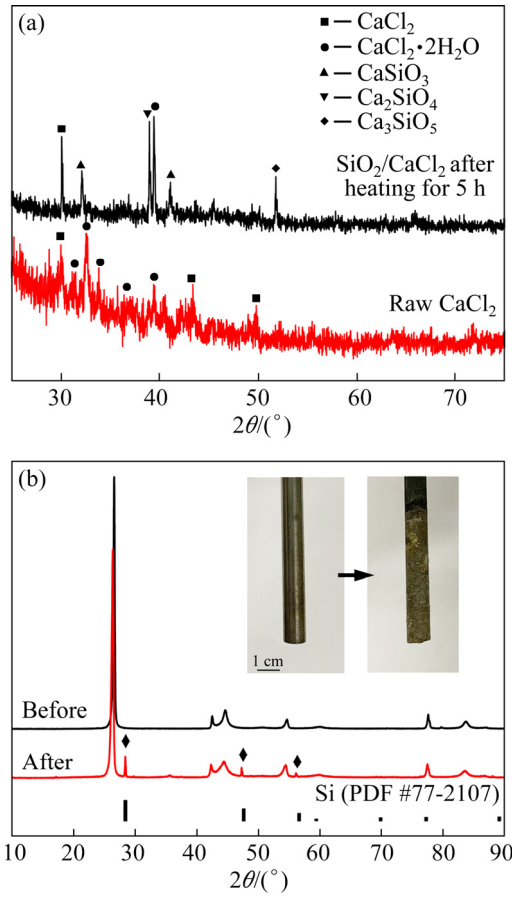

Fig. 4 XRD patterns of $CaCl_2$ and $SiO_2/CaCl_2$ mixtures after heating at 900 °C for 5 h (a); XRD patterns of graphite rod used as cathode before and after electrolysis in molten $SiO_2/CaCl_2$ (The inset is the corresponding digital photographs) (b)

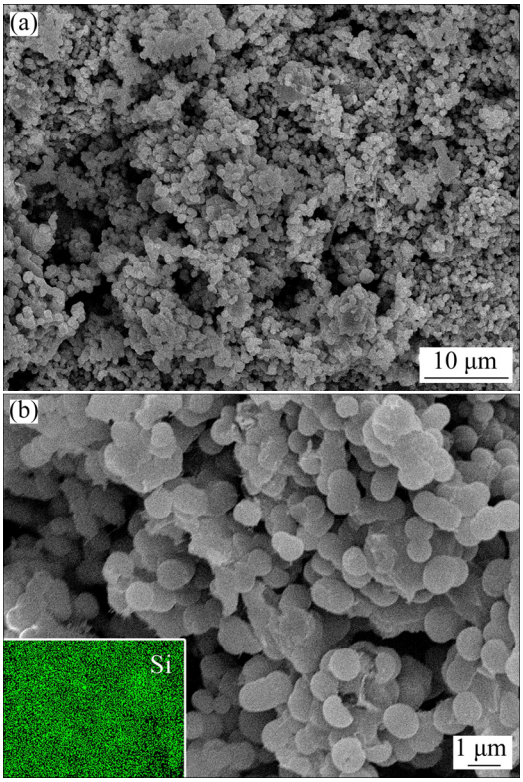

Fig. 5 SEM images of electrodeposited Si particles (The inset in (b) is its corresponding EDS mapping)

Based on the above results, a possible electrosynthesis mechanism for the preparation of SiC nanoparticles from SiO_2/C in molten $CaCl_2$ has been proposed, and its schematic diagram is shown in Fig. 6. Since $CaCl_2$ typically possesses some residual moisture and crystal water, it is challenging to completely eliminate these oxygen-contained impurities with heat-treatment and pre-electrolysis process [23,24]. Therefore, certain amounts of Ca^{2+} and O^{2-} may remain in the molten $CaCl_2$ due to the dissolution of calcium oxide (CaO) via Reactions (2)−(7). Therefore, when SiO_2/C pellet is immersed in the molten $CaCl_2$, SiO_2 can spontaneously react with CaO (Ca^{2+}, O^{2-}) to form Ca_xSiO_y (such as $CaSiO_3$ via Reaction (8)) through liquid-phase reaction. Meanwhile, SiO_2 and Ca_xSiO_y can be directly electro-reduced to Si via Reactions (9)−(11). The ionized O^{2-} may also participate in the combination reaction and result in the generation of Ca_xSiO_y during the migration process in the cathodic pellet. Since SiO_2 and C powders are supposedly well mixed, the resultant Si can spontaneously react with C to produce SiC via in-situ carbonization Reaction (12). Unlike the metal materials, semiconductor silicon does not possess enough delocalized electrons to provoke the thermal-induced strain behavior, and therefore is beneficial to the formation of micro/nanostructure silicon-based materials [9]. Furthermore, the generation of ultrafine SiC nanoparticles is also related to the utilization of nanometer-level raw material and massive and homogeneous nucleation behavior during the electrolysis process (Fig. 3).

$$CaCl_2{\cdot}2H_2O \rightarrow CaCl_2{\cdot}H_2O + H_2O(g) \quad (2)$$

$$CaCl_2{\cdot}H_2O \rightarrow CaCl_2 + H_2O(g) \quad (3)$$

$$CaCl_2{\cdot}H_2O \rightarrow CaClOH + HCl(g) \quad (4)$$

$$CaCl_2{\cdot}H_2O \rightarrow CaCl_2 + H_2O(g) \quad (5)$$

$$CaCl_2{\cdot}H_2O \rightarrow CaO + 2HCl(g) \quad (6)$$

$$CaO \rightarrow Ca^{2+} + O^{2-} \quad (7)$$

$$SiO_2 + CaO(Ca^{2+}, O^{2-}) \rightarrow CaSiO_3,\ \Delta G_{900\,^\circ C} = -90.802\ \text{kJ/mol} \quad (8)$$

$$SiO_2 + 4e \rightarrow Si(s) + 2O^{2-} \quad (9)$$

$$CaSiO_3 \rightarrow Ca^{2+} + SiO_3^{2-} \quad (10)$$

$$SiO_3^{2-} + 4e \rightarrow Si(s) + 3O^{2-} \quad (11)$$

$$Si(s) + C(s) \rightarrow SiC(s),\ \Delta G_{900\,^\circ C} = -62.396\ \text{kJ/mol} \quad (12)$$

3.3 Microstructure and photoluminescence property of synthesized SiC nanoparticles

The as-synthesized SiC powder was further characterized by TEM and high-resolution TEM (HR-TEM) to illustrate its detailed microstructure and property. As shown in Fig. 7, the synthesized SiC possesses irregular micromorphology of nanoparticles. Furthermore, the SiC nanoparticles are interconnected, as observed in Fig. 7(a), which indicates the existence of grain growth behavior during the formation of SiC. According to the previous works [20,25,26], Ostwald ripening is the main growth mechanism of Si-based materials, which involves the growth of large grains at the cost of small ones during the solution-precipitation process. Moreover, liquid molten salt featured with high polarity and surface tension can suppress particle agglomeration, and this may induce the formation of SiC nanoparticles [9]. The inset in Fig. 7(a) shows the selected area electron diffraction (SAED) pattern, where a set of concentric rings can be observed. Such a result

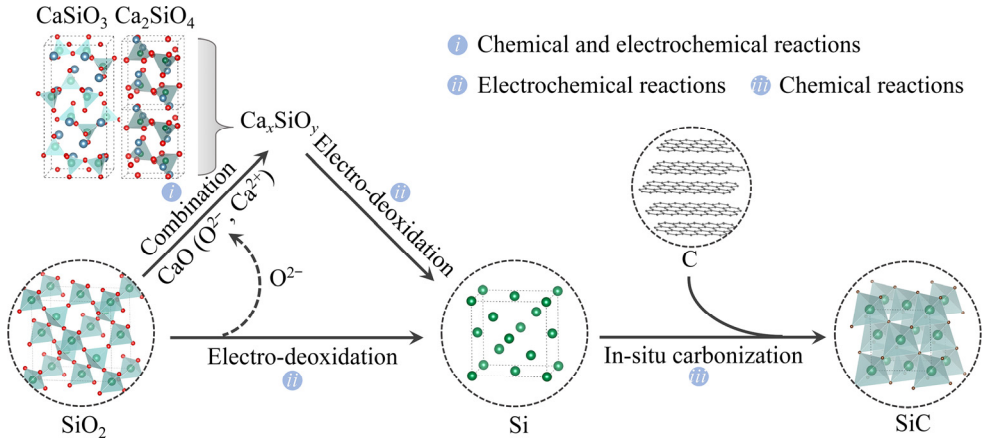

Fig. 6 Schematic diagram of electrosynthesis mechanism for preparation of SiC nanoparticles from SiO_2/C in molten $CaCl_2$

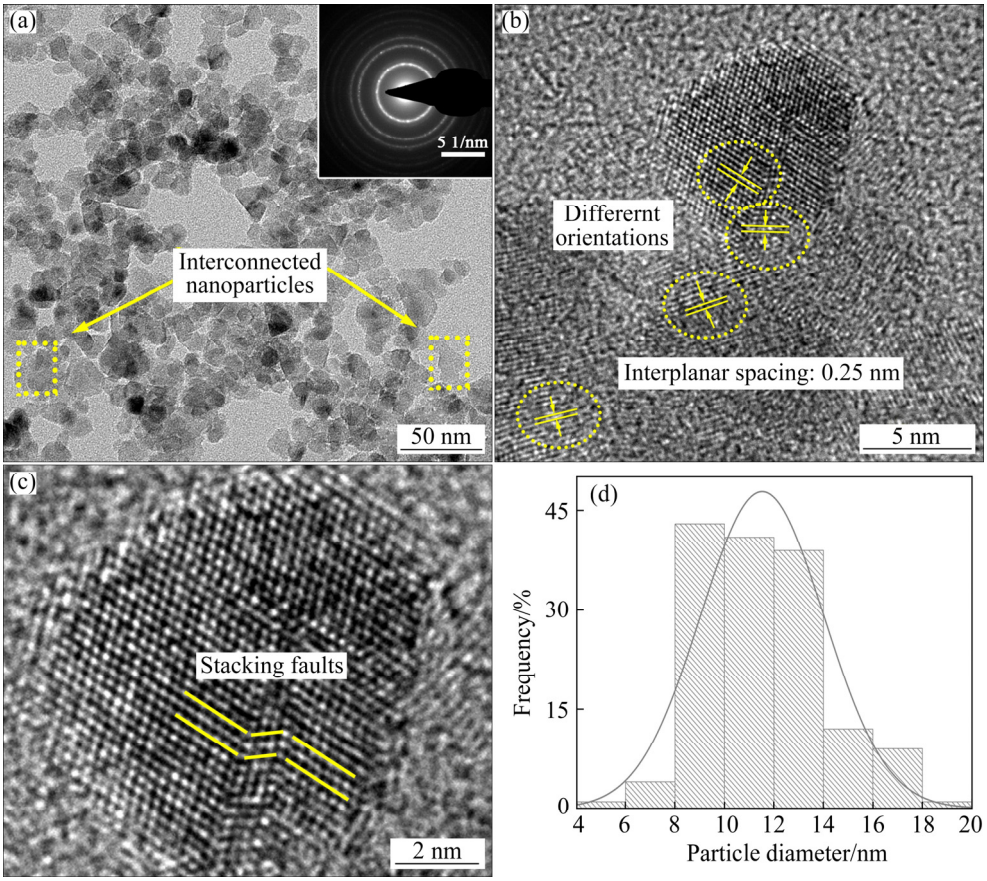

Fig. 7 TEM (a) and HR-TEM (b, c) images of as-synthesized SiC nanoparticles (The inset in (a) is its corresponding SAED pattern); Particle size distribution of SiC nanoparticles (d)

implies that the as-synthesized SiC nanoparticles possess a polycrystalline structure. The HR-TEM image (Fig. 7(b)) confirms that the interplanar spacing of SiC nanoparticles is about 0.25 nm, which corresponds to that of (111) plane of cubic β-SiC. Different grain orientations can also be observed in the inside and the junctions of SiC nanoparticles, illustrating the polycrystalline property of SiC. Furthermore, the SiC nanoparticles have some microstructural defects, such as stacking faults, as shown in Fig. 7(c). The particle size distribution calculated from the TEM image is displayed in Fig. 7(d). The results show that the particle size of the synthesized SiC is concentrated in the range of 8−14 nm.

Raman measurement was performed to further investigate the microstructure of the resultant SiC nanoparticles. As shown in Fig. 8(a), two broad peaks located at 783 and 945 cm^{-1} in the Raman spectrum are assigned to the transverse optical (TO) and longitudinal optical (LO) phonon modes of β-SiC, respectively. Compared to the bulk β-SiC Raman peak, the TO peak and LO peak of β-SiC nanoparticles shift towards the lower wavelength by 13 and 27 cm^{-1}, respectively, and these values close to the theoretical offsets are caused by quantum confined effects [27]. Furthermore, the intensity of TO peak is significantly higher than that of LO peak, which implies the presence of certain defects, e.g., dislocations, in the SiC nanoparticle [28]. Photoluminescence (PL) spectrum was measured with excitation at 252 nm at room temperature to investigate the optical properties of the as-synthesized SiC nanoparticles. As shown in Fig. 8(b), a strong emission peak located at about 410 nm can be observed in the PL spectrum. This emission peak shows an obvious blue-shift based on the previous works [29−31]. Since the particle size of the β-SiC synthesized in this work is about 10 nm, quantum confinement effects may be induced within the nano-material. In addition, some microstructural defects such as stacking faults are detected by the Raman spectrum and TEM micrograph (Fig. 7) in the SiC nanoparticles. Previous studies [31−33] speculated that distorted and weakly bonded atoms (e.g., Si—C, Si—Si)

with twisted bonding angle or longer bonding length can also cause the blue-shift emissions, which deserves further investigation. In general, the presence of quantum confinement effects and the microstructural defects of nano-scale SiC may result in the blue-shift phenomenon observed in the PL spectrum [30]. Based on the above results, it is confirmed that the impressive optical property enables the synthesized SiC nanoparticles to be potentially employed in the optoelectronic field.

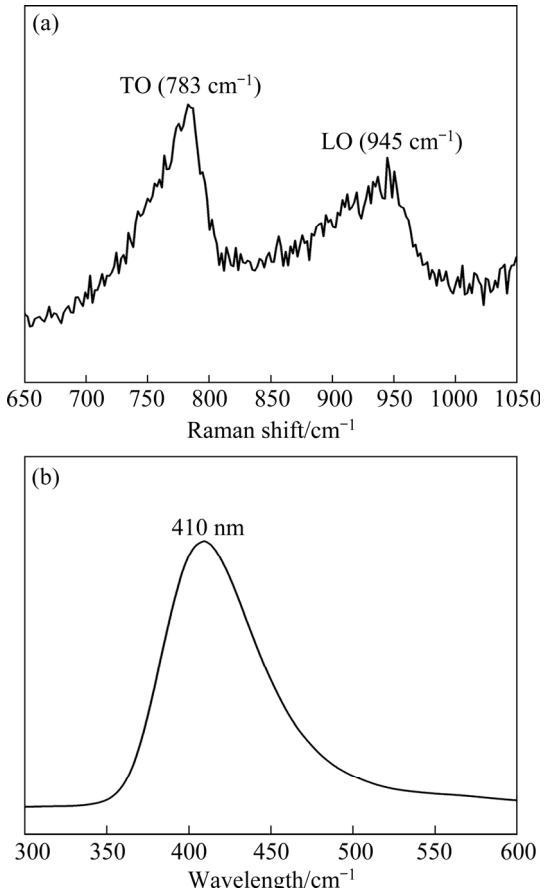

Fig. 8 Raman (a) and photoluminescence (b) spectra of synthesized SiC nanoparticles

4 Conclusions

(1) SiC nanoparticles has been electrochemically synthesized from mixed SiO_2 and C powders at 900 °C in molten $CaCl_2$.

(2) The electrochemical synthesis mechanism of SiC mainly involves the generation of intermediate products of Ca_xSiO_y through a combined chemical/electrochemical process, the electrochemical deoxidation of SiO_2 and Ca_xSiO_y, and in-situ carbonization reaction between resultant Si and C.

(3) The as-synthesized SiC possesses the morphology of irregular nanoparticles with particle size ranging from 8 to 14 nm. The microstructure of the SiC exhibits polycrystalline cubic β-phase structure and some microstructural defects, such as stacking fault.

(4) The SiC nanoparticles demonstrate obvious quantum-confined effects, and show remarkable photoluminescence property due to the synergetic size effect and microstructural characteristics.

Acknowledgments

This work was financially supported by the National Natural Science Foundation of China (Nos. 52022054, 51974181, 52004157), the Shanghai Rising-Star Program, China (No. 19QA1403600), the Shanghai Sailing Program, China (No. 21YF1412900), and the Iron and Steel Joint Research Fund of National Natural Science Foundation of China and China Baowu Steel Group Corporation Limited (No. U1860203). The authors also thank the Program for Professor of Special Appointment (Eastern Scholar) at Shanghai Institutions of Higher Learning, China (No. TP2019041), the Shanghai Postdoctoral Excellence Program, China (No. 2021160), and the "Shuguang Program" supported by the Shanghai Education Development Foundation and the Shanghai Municipal Education Commission, China (No. 21SG42).

References

[1] FAN Ji-yang, LI Hong-xia, LIANG Jiang, SO L K Y, LAM Y W, CHU P K. 3C−SiC nanocrystals as fluorescent biological labels [J]. Small, 2008, 4: 1058−1062.

[2] SINGH R K, TELANG A, DAS S. Microstructure, mechanical properties and two-body abrasive wear behaviour of hypereutectic Al−Si−SiC composite [J]. Transactions of Nonferrous Metals Society of China, 2020, 30: 65−75.

[3] ZHANG Guang-qiang, WEI Guo-dong, ZHENG Ke-zhi, LI Liang, XU Da-peng, WANG De-yong, XUE Yan-feng, SU Wen-hui. The synthesis of β-SiC nanoparticles by high-energy mechanical ball milling and their photoluminescence properties [J]. Journal of Nanoscience and Nanotechnology, 2010, 10: 1951−1955.

[4] SOMOGYI B, ZOLYOMI V, GALI A. In introducing color centers to silicon carbide nanocrystals for in vivo biomarker applications: A first principles study [J]. Materials Science Forum, 2013, 740/741/742: 641−644.

[5] HENDERSON E J, VEINOT J G. From phenylsiloxane polymer composition to size-controlled silicon carbide nanocrystals [J]. Journal of the American Chemical Society,

2009, 131: 809−815.

[6] XIE Xiang-min, SU Zhe-an, HUANG Dong, YANG Cheng, WANG Ya-feng, JIANG Ding-yu, HUANG Qi-zhong. Synthesis and growth mechanism of SiC/SiO_2 nanochains by catalyst-free thermal evaporation method in Ar/CO atmosphere [J]. Transactions of Nonferrous Metals Society of China, 2020, 30: 3058−3066.

[7] KIM D, KIM D Y, KWON J H, KIM K S, HWANG N M. Generation of charged SiC nanoparticles during HWCVD process [J]. Electronic Materials Letters, 2020, 16: 498−505.

[8] SHUAIB E, YOGESH G K, SASTIKUMAR D. Amorphous and photoluminescent crystalline silicon carbide nanoparticles synthesized by laser ablation in liquids [J]. Materials Today: Proceedings, 2020, 50: 2745−2750.

[9] XIAO Wei, WANG Xin, YIN Hua-yi, ZHU Hua, WANG Di-hua. Verification and implications of the dissolution–electrodeposition process during the electro-reduction of solid silica in molten $CaCl_2$ [J]. RSC Advances, 2012, 2: 7588−7593.

[10] PANG Zhong-ya, LI Guang-shi, XIONG Xiao-lu, JI Li, XU Qian, ZOU Xing-li, LU Xiong-gang. Molten salt synthesis of porous carbon and its application in supercapacitors: A review [J]. Journal of Energy Chemistry, 2021, 61: 622−640.

[11] CHEN G Z, FRAY D J, FARTHING T W. Direct electrochemical reduction of titanium dioxide to titanium in molten calcium chloride [J]. Nature, 2000, 407: 361−364.

[12] ZOU Xing-li, JI Li, LU Xiong-gang, ZHOU Zhong-fu. Facile electrosynthesis of silicon carbide nanowires from silica/carbon precursors in molten salt [J]. Scientific Reports, 2017, 7: 9978.

[13] XIAO Wei, JIN Xian-bo, CHEN G Z. Up-scalable and controllable electrolytic production of photo-responsive nanostructured silicon [J]. Journal of Materials Chemistry A, 2013, 1: 10243−10250.

[14] LI Shao-long, LIU Yang, CHE Yu-si, SONG Jian-xun, SHU Yong-chun, HE Ji-lin, XU Bao-qiang, Yang Bin. Recycling of spent indium–gallium–zinc oxide based on molten salt electrolysis [J]. ACS Sustainable Chemistry & Engineering, 2020, 8: 16296−16303.

[15] WENG Wei, ZENG Chen, XIAO Wei. In situ pyrolysis concerted formation of Si/C hybrids during molten salt electrolysis of SiO_2@polydopamine [J]. ACS Applied Materials & Interfaces, 2019, 11: 9156−9163.

[16] LIU Zheng-wei, ZHANG Hong-ling PEI Li-li, SHI Yi-lang, CAI Zai-hua, XU Hong-bin, ZHANG Yi. Direct electrolytic preparation of chromium metal in $CaCl_2$−NaCl eutectic salt [J]. Transactions of Nonferrous Metals Society of China, 2018, 28: 376−384.

[17] XIAO Wei, JIN Xian-bo, DENG Yuan, WANG Di-hua, HU Xiao-hong, CHEN G Z. Electrochemically driven three-phase interlines into insulator compounds: Electroreduction of solid SiO_2 in molten $CaCl_2$ [J]. ChemPhysChem, 2006, 7: 1750−1758.

[18] CZECH B, HOJAMBERDIEV M, BOGUSZ A. Impact of thermal treatment of calcium silicate-rich slag on the removal of cadmium from aqueous solution [J]. Journal of Cleaner Production, 2018, 200: 369−379.

[19] ZOU Xing-li, CHEN Chao-yi, LU Xiong-gang, LI Shang-shu, XU Qian, ZHOU Zhong-fu, DING Wei-zhong. Solid oxide membrane (SOM) process for facile electrosynthesis of metal carbides and composites [J]. Metallurgical and Materials Transactions B, 2016, 48: 664−677.

[20] ZOU Xing-li, JI Li, PANG Zhong-ya, XU Qian, LU Xiong-gang. Continuous electrodeposition of silicon and germanium micro/nanowires from their oxides precursors in molten salt [J]. Journal of Energy Chemistry, 2020, 44: 147−153.

[21] ZOU Xing-li, JI Li, GE Jian-bang, SADOWAY D R, YU E T, BARD A J. Electrodeposition of crystalline silicon films from silicon dioxide for low-cost photovoltaic applications [J]. Nature Communications, 2019, 10: 5772.

[22] DONG Yi-fan, SLADE T, STOLT M J, LI Lin-sen, GIRARD S N, MAI Li-qiang, JIN Song. Low-temperature molten-salt production of silicon nanowires by the electrochemical reduction of $CaSiO_3$ [J]. Angewandte Chemie International Edition, 2017, 56: 14453−14457.

[23] PANG Zhong-ya, ZOU Xing-li, TANG Wei, SHI Tian-yu, WANG Shu-juan, JI Li, HSU H Y, XU Qian, LU Xiong-gang. Electrosynthesis of Ti_3AlC_2-derived porous carbon in molten salt [J]. JOM, 2020, 72: 3887−3894.

[24] XU Bao-qiang, YANG Bin, JIA Jin-gang, LIU Da-chun, XIONG Heng, DENG Yong. Behavior of calcium chloride in reduction process of titanium dioxide by calcium vapor [J]. Journal of Alloys and Compounds, 2013, 576: 208−214.

[25] NARUMI T, CHAUSSENDE D, YOSHIKAWA T. 3C-, 4H-, and 6H-SiC crystal habitus and interfacial behaviours in high temperature Si-based solvents [J]. CrystEngComm, 2020, 22: 3489−3496.

[26] ROGER J, le PETITCORPS Y. Microstructural evolution of SiC powder in molten silicon [J]. Ceramics International, 2018, 44: 19836−19845.

[27] ZHANG Shu-lin, ZHU Bang-fen, HUANG Fu-ming, YAN Yan, SHANG Er-yi, FAN Shou-shan, HAN Wei-giang. Effect of defects on optical phonon Raman spectra in SiC nanorods [J]. Solid State Communications, 1999, 111: 647−651.

[28] BECHELANY M, BRIOUDE A, CORNU D, FERRO G, MIELE P. A Raman spectroscopy study of individual SiC nanowires [J]. Advanced Functional Materials, 2007, 17: 939−943.

[29] LIU Rong-zheng, LIU Ma-lin, CHANG Jia-xing. Large-scale synthesis of monodisperse SiC nanoparticles with adjustable size, stoichiometric ratio and properties by fluidized bed chemical vapor deposition [J]. Journal of Nanoparticle Research, 2017, 19: 26.

[30] JIANG Sheng-nan, GAO Shuai-bo, KONG Jian, JIN Xing, WEI Dong-hui, LI Da-gang, XING Peng-fei. Study on the synthesis of β-SiC nanoparticles from diamond-wire silicon cutting waste [J]. RSC Advances, 2019, 9: 23785−23790.

[31] ZHANG Ju, LI Wei, JIA Quan-li, LIN Liang-xu, HUANG Jun-tong, ZHANG Shao-wei. Molten salt assisted synthesis of 3C−SiC nanowire and its photoluminescence properties [J]. Ceramics International, 2015, 41: 12614−12620.

[32] WU Ren-bing, LI Bao-sheng, GAO Ming-xia, CHEN Jian-jun, ZHU Qi-miao, PAN Yi. Tuning the morphologies of SiC nanowires via the control of growth temperature, and their

photoluminescence properties [J]. Nanotechnology, 2008, 19: 335602.
[33] SHAJAHAN M, MO Y, NAHM K S. Effect of chemical vapor deposition energy sources on the structure of SiC prepared by carbon nanotubes-confined reaction [J]. Journal of Vacuum Science & Technology B, 2003, 9: 1149−1156.

熔盐电解合成碳化硅纳米颗粒及其光致发光特性

庞忠亚[1]，李 想[1]，张学强[1]，李金键[1]，汪淑娟[1]，
熊晓璐[1]，李光石[1]，许 茜[1]，周忠福[1,2]，邹星礼[1]，鲁雄刚[1,3]

1. 上海大学 材料科学与工程学院 高品质特殊钢冶金与制备省部共建国家重点实验室，上海 200444；
2. Institute of Mathematics and Physics, Aberystwyth University, Aberystwyth SY23 3BZ, UK;
3. 上海电机学院 材料学院，上海 201306

摘 要：提出一种一步熔盐电化学方法，以超细二氧化硅和碳粉混合物为原料合成碳化硅纳米颗粒。通过 X 射线衍射、电子显微镜、拉曼光谱、光致发光光谱等系统研究电解合成过程及产物的物化特性。提出二氧化硅/碳粉在氯化钙熔盐中电解合成纳米碳化硅时存在化学/电化学复合、电化学脱氧和原位碳化的耦合反应机理。结果表明，所制备的碳化硅纳米颗粒的粒径集中分布在 8~14 nm，并具有多晶结构。此外，由于协同的尺寸效应和微观结构特征，碳化硅纳米颗粒具有明显的光致发光特性。

关键词：碳化硅；纳米材料；熔盐电解；脱氧；光致发光

(Edited by Bing YANG)